

Search range in experimental quantum annealing

Nicholas Chancellor and Viv Kendon

*Department of Physics; Joint Quantum Centre (JQC) Durham-Newcastle
Durham University, South Road, Durham, DH1 3LE, UK*

(Dated: March 22, 2022)

We construct an Ising Hamiltonian with an engineered energy landscape such that it has a local energy minimum which is near to the true global minimum solution, and further away from a false minimum. Using a technique established in previous experiments, we design our experiment such that (at least on timescales relevant to our study) the false minimum is reached preferentially in forward annealing due to high levels of quantum fluctuations. This allows us to demonstrate the key principle of reverse annealing, that the solution space can be searched locally, preferentially finding nearby solutions, even in the presence of a false minimum. We perform these experiments on two flux qubit quantum annealers, one with higher noise levels than the other. We find evidence that the lower noise device is more likely to find the more distant energy minimum (the false minimum in this case), suggesting that reducing noise fundamentally increases the range over which flux qubit quantum annealers are able to search. Our work explains why reducing the noise leads to improved performance on these quantum annealers. This supports the idea that they may be able to search over broad regions of the solution space quickly, one of the core reasons why quantum annealers are viewed as a potential avenue for a quantum computational advantage.

Introduction and background

Quantum annealing, an approach to quantum computing where optimisation and other problems are mapped directly to the ground and low energy states of a Hamiltonian and quantum fluctuations are used to solve the problem, has been a subject of much interest recently. They are potential candidates to solve a wide variety of real problems, with applications as diverse as cryptography [1], design of radar waveforms [2], protein folding [3], air traffic control [4], scheduling [5–7], and hydrology [8].

A driving force behind interest in quantum annealing is the development of large scale superconducting flux qubit quantum annealers. While it is possible to build quantum annealers using other technologies such as trapped atoms [9], by far the largest and most technologically mature quantum annealing devices currently available are the superconducting flux qubit quantum processing units (QPUs) produced by D-Wave Systems Inc., which are the subject of the experiments described here. In these devices, the low energy subspace of superconducting flux qubits is used to implement an Ising Hamiltonian described by a coupling matrix J and a field vector h , which is subject to quantum fluctuations which flip single bits. The total effective Hamiltonian can be expressed as a transverse Ising Hamiltonian,

$$H(s) = -A(s) \sum_i \sigma_i^x + B(s) \left(\sum_{i,j \in \chi} J_{i,j} \sigma_i^z \sigma_j^z \sum_i h_i \sigma_i^z \right), \quad (1)$$

where $\sigma_i^{x(z)}$ is the Pauli $x(z)$ spin operator acting on qubit i , and $A(s)$ and $B(s)$ are time dependent real parameters. The annealing parameter $0 \leq s \leq 1$ controls the schedule such that in a traditional annealing protocol $s \propto t$. This parameterization is chosen so that reverse annealing protocols can be more easily described math-

ematically. In this paper, we choose a convention where J_{ij} and h_i from Eq. (1) are dimensionless, while the control parameters, A, B have dimensions of frequency. Coupling between pairs of qubits is restricted to a graph χ determined by the hardware. A quantum annealing protocol is specified by the variation in time of the annealing parameters A and B . Traditional quantum annealing is performed by starting the system in an equal positive superposition of all computational basis states with $\frac{A}{B} \gg 1$ and varying the parameters continuously until $\frac{A}{B} \ll 1$. In principle, in the absence of noise, and if the parameters are changed slowly enough, this protocol finds the solution state with a probability approaching one. In practice, the noise on the QPUs cannot be neglected, so the picture of how they operate is significantly more complicated. However, given that the dominant noise source on these devices is coupling to the low temperature substrate of the qubits, the net effect of noise is not always detrimental. This is emphasized by the result in [10], where it was found that thermal fluctuations can lead to a large enhancement of success probability over what is expected from a purely adiabatic protocol run over short timescales.

Since late 2017, a new protocol has become available to users of D-Wave devices, known as reverse annealing [11]. The QPU is initialized in a user defined computational basis state, with $\frac{A}{B} \ll 1$. The parameters are then changed to $\frac{A}{B} \sim 1$ to allow quantum fluctuations. Finally, the parameters are switched back to $\frac{A}{B} \ll 1$, so each qubit can be measured.

These protocols were motivated by the idea that a quantum annealer could be a more useful algorithmic tool if it were able to incorporate known information, either from classical algorithms, or from previous annealing runs [12]. Since the introduction of the reverse annealing feature, there have indeed been promising experimental results. These include: quantum simulation of the cel-

celebrated Kosterlitz-Thouless phase transition [13] which would not have been possible with traditional forward annealing; experiments showing that seeding the protocol with the result of a classical greedy search may improve portfolio optimisation [14]; evidence that repeated reverse anneals can improve performance in matrix factorization, [15, 16]; and evidence that reverse annealing calls can improve genetic algorithms [17]. While these results are highly promising, they all focus on the improvements which reverse annealing can provide, rather than verifying that it actually searches locally, as predicted. In this paper we fill this gap by verifying that reverse annealing does indeed perform the kind of local search predicted in [12]. The reverse annealing protocol, as it has been implemented on these devices, fundamentally relies on dissipation to find low energy states. If all noise was removed and these protocols were run adiabatically starting from a unique classical basis state, they would return to the state in which they were initialized. If run non-adiabatically, the protocol would incorporate nearby states, but there is no apparent mechanism for such a protocol to preferentially reach higher quality solution states, as there is for traditional non-adiabatic protocols [18]. There are other biased search protocols which work in the adiabatic limit [19–21], and recent work [18] suggests that the protocol explored in [20, 21] will also perform well far from the adiabatic, limit in the rapid quench regime.

Since dissipation plays such an important role in the reverse annealing protocols studied here, they are a natural tool for studying the effect of noise. The underlying protocol is very similar to the one used in macroscopic resonant tunnelling experiments [22] to characterize noise on flux qubits. Our experiments are not intended to examine single resonant tunnelling events, rather, they test the range of the local search which the annealer performs at two different noise levels, corresponding to the two different QPUs we are able to access. What we find is that, when the noise is reduced, the effective range of the local search is increased. Long range quantum tunnelling is a key feature of quantum annealers, that may one day allow them to obtain a quantum advantage. The increased range we observe here is a sign of the beneficial effects of noise reduction on quantum annealers. It also provides an explanation for the improved performance on the lower noise QPU observed in [23].

I. EXPERIMENTAL SETUP

The D-Wave Systems programmable annealer that we used has a reverse annealing capability that works as follows. The annealing parameters A and B are defined to be functions which depend on a single parameter s , which is in turn time dependent. The functional dependence of $A(s)$ and $B(s)$ is known [32] but is non-linear and dependent on the physical device parameters. A key feature is that A and B are both monotonic in s , decreasing and in-

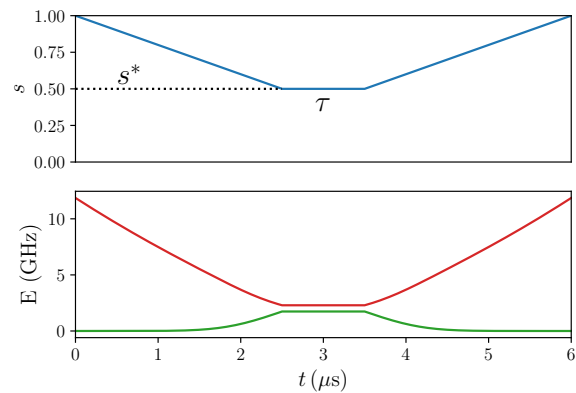


Figure 1: Top: Plot of s versus time for a reverse annealing protocol in which the device is annealed at the maximum allowed rate (requiring $5 \mu\text{s}$ to traverse the entire schedule), with a hold time τ of $1 \mu\text{s}$ and $s^* = 0.5$. Bottom: The A and B energy scales of this protocol performed on the low noise QPU model (see Fig. 2 and associate discussion in the main text). The red curve starting from around 10 GHz is B , the green curve starting at around 0 GHz is A .

creasing respectively, $A(s_1) > A(s_2)$ and $B(s_1) < B(s_2)$, if $s_1 > s_2$. An initial state is pre-programmed into the annealer with control parameter $s = 1$. The control parameter s is then linearly reduced until a value $s = s^*$ is reached, where the annealing protocol is paused for a period τ . The protocol is finished by annealing back to $s = 1$, and read out is performed normally. An example of a reverse annealing protocol is depicted in Fig. 1.

These experiments were performed in a period of 2019 during which a new model of QPU was being introduced, which had been re-engineered to reduce the noise. During this period, the older, higher noise model was still available to use, allowing a unique opportunity to experimentally study the effect of noise on these devices.

As depicted in Fig. 2, the high and low noise QPUs have different annealing schedules, so directly comparing behaviour at the same value of s does not provide a fair comparison. We instead define a single parameter $\Gamma(s) = A(s)/B(s)$

which encodes the ratio of fluctuation terms to problem Hamiltonian terms: this allows the results from the two devices to be compared on an equal footing.

A. Energy landscape design

Since the goal of this experiment is to study local searches of solution spaces of optimisation problems, we construct a Hamiltonian where the energy landscape has the following features:

1. a broad false energy minimum which will be found with high probability using a traditional forward annealing protocol;
2. a narrow true minimum;

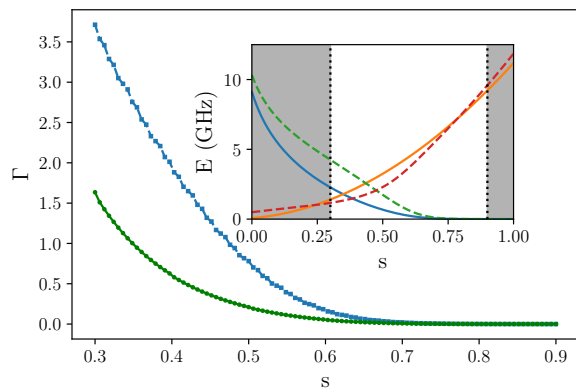


Figure 2: Ratio $\Gamma(s) = A(s)/B(s)$ for the high and low noise QPU at different values of s within the range of interest. Blue squares (green circles) represent the different values of $\Gamma^* = \Gamma(s^*)$ used for the low (high) noise QPU. Inset: A and B curves for the higher (solid lines with A in blue and B in gold) and lower (dashed lines with A in green and B in red) noise QPUs. Greyed out areas fall outside of the range of interest, either because Γ is very high and the system decays to its global ground state very rapidly, or because Γ is very low and the dynamics are effectively frozen.

3. a local energy minimum (starting state) which sits relatively near (in Hamming distance) to the true minimum and far from the false minimum;
4. controllable barrier height between the starting state and the true minimum.

Hamiltonians with the first two of these features are already known, and have been used experimentally in [10, 24]. We adapt the Hamiltonian used in [10] to include a local minimum for the starting state. The Hamiltonian we use, along with the the starting state, the unique state defining the true minimum, and the manifold of states which comprise the false minimum, are all represented pictorially in Fig. 3.

Transitioning from the starting state (Fig. 3 middle) to the true minimum energy state (Fig. 3 top) can be achieved by flipping the state of only four qubits. Furthermore, if the two qubits on the outer ring are flipped first, the system only needs to pass through one state which has higher energy than the initial value. This higher energy state has the two qubits on the inner ring taking their initial value, but the two on the outer ring disagreeing, and this state will only have $2 J_t$ more energy than the initial state. If $J_t = 0$, the true minimum can be reached without passing through any higher energy states.

On the other hand, to reach the false minimum (Fig. 3 bottom) from either the starting state or the true minimum, six spins on the inner rings need to be flipped, and the system must pass through states with a higher energy than the initial value regardless of the value of J_t . Compared to the transition between the starting state and the true minimum, more bit flips are required, and

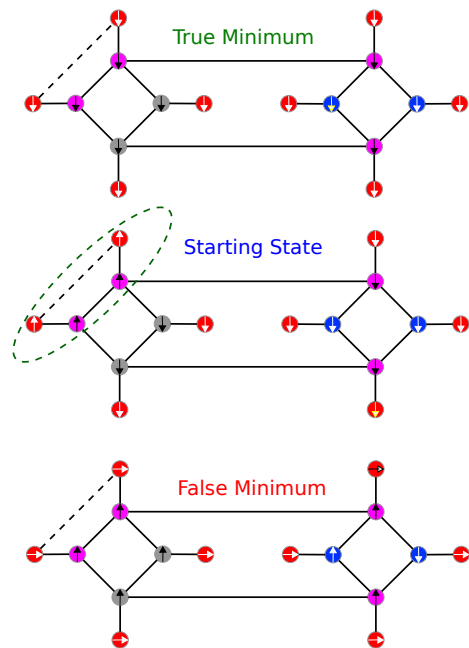


Figure 3: The Hamiltonian used in the experiment and the three relevant sets of states, the true minimum (top), the starting state (middle), and the manifold of states which comprise the false minimum (bottom). Solid edges represent ferromagnetic couplings of unit strength ($J = -1$), the dashed edge represents a tunable ferromagnetic coupling with strength $|J| = J_t$. The red circles on the outer ring represent qubits with fields $h = +1$, the four purple circles in the inner ring have $h = -1$, the two dark blue circles have $h = -1.95$, and the two light grey circles have $h = 0$. Arrows indicate the state of the qubit, with up (down) arrows representing $|0\rangle$ ($|1\rangle$), horizontal arrows representing superpositions of computational basis states which may be measured as either $|0\rangle$ or $|1\rangle$. The green dashed oval is a guide to the eye to show which qubits are flipped between the starting state and the true minimum energy state.

the system needs to pass through more than one state with a higher energy than the starting state. It is thus fair to characterize the transition between the starting state and the false minimum as being longer range (in Hamming distance) than the transition to the true minimum.

From summing the energy contributions from fields and couplers (and assuming that the two qubits coupled by the coupler with strength J_t take the same value in the case of the false minimum), we see that the expectation value of the true and false minimum with respect to the dimensionless Hamiltonian H_{prob} only differs by 0.2. This implies that an avoided crossing between the true and false minima will occur relatively late in a traditional anneal, when the transverse field is very weak

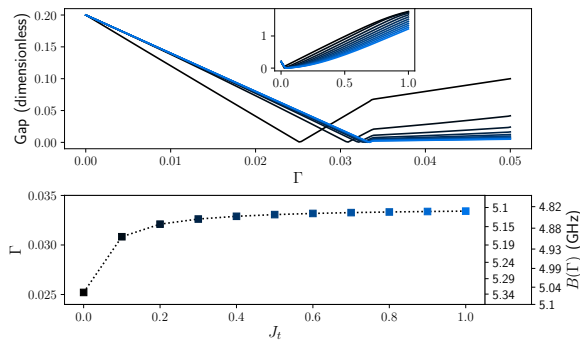


Figure 4: Upper: dimensionless gap versus Γ , for different values of J_t , as colour coded in the lower plot. Inset: same figure plotted on a larger scale. Lower: position of the crossing versus J_t , the dimensionless ratio Γ is on the left axis, while the values of $B(\Gamma)$ corresponding to these Γ values for the different QPUs is given on the right axes, with the inner (outer) axis representing the lower (higher) noise model.

and the time scale for resonant tunnelling will be very long. This is by design, since our experiment is intended to study local search around the starting state, not resonant tunnelling between the two minima. We can confirm this numerically, to rule out the possibility of resonant tunnelling between the true and false minima. Fig. 4 depicts the energy gap between the ground and first excited state around the avoided crossing for different values of J_t . Due to the closeness of the avoided crossing, we were not able to extract the exact gap values, but were able to numerically upper bound the minimum dimensionless gap to be of the order 10^{-9} , using bisection based on numerical derivatives, for all values of J_t . This implies that the gap will be of the order $10^{-9}B(s\{\Gamma\})$, where $s\{\Gamma\}$ is defined as the value of s corresponding to Γ . The monotonicity of $A(s)$ and $B(s)$ implies that $\Gamma(s)$ will also be monotonic, and therefore $s\{\Gamma\}$ will be uniquely defined. From Fig. 4, we see that $B(s\{\Gamma\})$ is of the order of GHz around the crossing point, for both the higher and lower noise QPUs. This means that the timescale related to resonant tunnelling can be lower bounded to a range of hundreds of milliseconds to seconds. Since the longest hold time used in our experiments ($100 \mu\text{s}$) is at least 1,000 times smaller than this lower bound, we can safely conclude that resonant tunnelling directly between the true and false minimum is not playing a meaningful role in our experiments. This does not preclude non-resonant tunnelling at larger Γ values, the indirect thermally assisted processes observed in [10], or other complex processes involving more than two energy levels. Ruling out direct resonant tunnelling is important because it provides a contrast between our experiment and [25], where reduced noise on the QPU leads to an increase in single and multi qubit macroscopic resonant tunnelling rates.

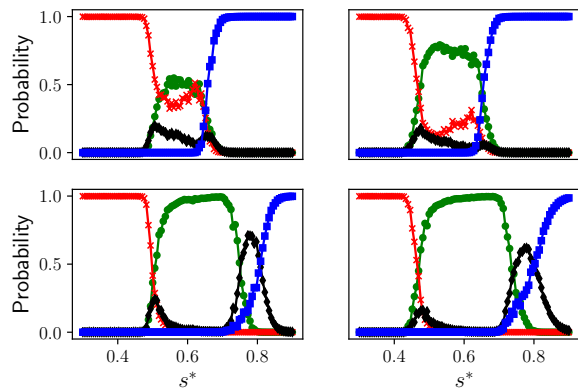


Figure 5: Probability of the system to be in different states at the end of the anneal versus s^* for lower and higher noise QPUs and different local barrier heights set by J_t . Top row: $J_t = 1$, bottom row: $J_t = 0$, left (right) column: lower (higher) noise QPU. Probability to be in the initial state (blue squares), the true minimum energy state (green circles), the false minimum energy state (red crosses), and any other state (black diamonds). All data in these plots were taken with a hold time of $\tau = 5 \mu\text{s}$. Note that the schedules are different for the two QPUs, so a direct comparison at the same value of s^* is not immediately meaningful; this plot uses s^* rather than Γ^* so that the behaviour at large s^* is more readily visible. Statistical error bars are smaller than the symbols.

II. RESULTS

A. Local search by reverse annealing

We first show that the results from the experiments reported here demonstrate that the reverse annealing protocol does indeed perform searches locally in solutions space, as argued in [12]. It is valuable to directly verify this behaviour experimentally in small systems. In this setting, what we expect is that for intermediate values of s^* (equivalently, intermediate Γ^*), the system should find the true minimum with reasonable probability. In contrast, for too large a value of s^* (small Γ^*), the system will remain frozen in its initial state, and for too small a value of s^* (large Γ^*), the system will search the solution space globally and become trapped in the false minimum. Fig. 5 shows that this is indeed the case for both QPUs. For intermediate values of $0.5 \lesssim s^* \lesssim 0.7$, the true minimum (green) is found preferentially. Above and below this range, the initial state (blue) and false minimum (red) are observed respectively, with near unit probability. If $J_t = 0$ then no energy barrier needs to be overcome to transfer from the starting state to the true minimum and therefore nearly all of the probability amplitude is able to be transferred. A large peak in the probability to be in a state which is neither the true minimum, the false minimum, nor the starting state can also be observed for some values of s^* at the edges of the range, $s^* \simeq 0.5$ and $s^* \simeq 0.7$. This is likely due to slow dynamics leading to the system becoming stuck in

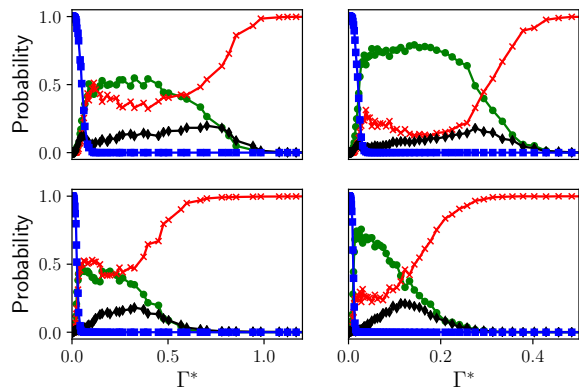


Figure 6: Probability of the system to be in different states versus s^* for lower and higher noise QPUs and two different hold times τ . Top row: $\tau = 5 \mu\text{s}$, bottom row: $\tau = 100 \mu\text{s}$, left (right) column: lower (higher) noise QPU. Probability to be in the initial state (blue squares), the true minimum energy state (green circles), the false minimum energy state (red crosses), and any other state (black diamonds). All plots here are for $J_t = 1$. Statistical error bars are smaller than the depicted symbols.

a state intermediate between the starting state and the true minimum.

A larger barrier $J_t = 1$ seems to trap the amplitude in the initial state until a relatively smaller value of s^* is used. This leads to less than 100% of the probability in the true minimum since at smaller s (larger Γ), the amplitude is able to tunnel to the false minimum more effectively. This feature is more pronounced in the lower noise QPU.

The plots in Fig. 5 are all for a fixed hold time $\tau = 5 \mu\text{s}$ (see Fig. 1). The effect of varying the hold time τ is shown in Fig. 6, which is plotted against Γ^* instead of s^* . The top row shows the same data as the top row of Fig. 5, while the bottom row is for hold time $\tau = 100 \mu\text{s}$. Longer hold times reduce the value of Γ^* (equivalently, increase s^*) above which the system is no longer found in the global minimum, and also reduce the value of Γ^* (increase s^*) at which the system leaves the initial state. Both of these effects make intuitive sense, as the system is more likely to transition to a lower energy state given more time. Two further observations are also worth making. Firstly, the QPU with higher noise levels makes these transitions at lower values of Γ^* than the QPU with lower noise levels (note the different scales for Γ^* in Fig. 6). This again makes intuitive sense. The computation is driven by thermal dissipation mediated by coupling between the substrate of the QPU and the qubits. This coupling will be stronger in the higher noise QPU, and therefore the timescales associated with dissipation will be shorter, allowing dissipation to happen at lower values of Γ^* for the same hold time τ . Secondly, the peak value of the probability to be found in the true minimum is very similar for both hold times. This suggests that, at relatively low Γ^* (but still large enough

to leave the initial state), the timescale associated with transferring from the true minimum to the false minimum is much longer than even the longest hold time of $\tau = 100 \mu\text{s}$. Thus, we have a picture of fast transfer out of the initial state, followed by relatively slow transfer between the other minima. Furthermore, the initial transfer strongly favours the nearby true minimum over the false minimum further away. This demonstrates that the reverse annealing protocol does indeed search the solution space locally, validating the conceptual argument that the performance increases seen in reverse annealing protocols are due to an ability to preferentially search locally in promising areas of the solution space.

B. Search range and noise levels

Having demonstrated that reverse annealing performs a local search on QPUs with both higher and lower noise levels, we now look at the differences in the behaviour of the two devices. We have already observed two basic effects. Firstly, the effective timescale for transferring between states is shorter for the higher noise QPU. Secondly, and more interestingly, we observe that the low noise system appears to have a relatively higher probability to transfer amplitude to the false minimum, which is further in Hamming distance from the initial state than the true minimum. Although in this engineered problem, this means that the probability of “success” is lower in our experiment, it hints at something very important, namely that the transfer between states has a longer range character in the lower noise QPU. The use of quantum coherence for long range exploration of a solution space is one of the attributes which should be able to give quantum annealing an advantage over classical methods. It is thus worth examining the search range on both QPUs more carefully.

First, we examine what happens as we change J_t , the strength of the barrier between the initial state and the true minimum. As Fig. 7 illustrates, the probability to reach the true solution (and therefore not end up in the false minimum) is roughly the same for both QPUs if the barrier between the initial state and true solution state is small. The behaviour of the two QPUs starts to diverge around $J_t = 0.4$, with the higher noise QPU showing a lower probability of finding the true minimum for $J_t > 0.4$. This intuitively makes sense: without a barrier preventing rapid decay into the true minimum, this decay will happen before Γ is large enough to reach the false minimum. As Fig. 8 demonstrates, the state is tunnelling into the false minimum preferentially on the lower noise device, indicating a longer range character to the search.

We now more carefully examine the effect of the hold time τ on the peak probability to be found in the true minimum. As the data in the previous section suggest, the peak value seems to be unaffected by the hold time, consistent with a separation of time scales between tun-

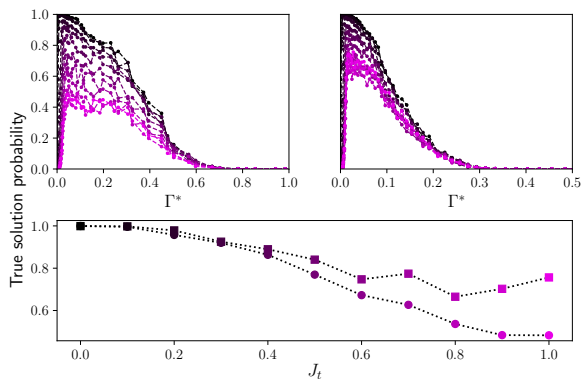


Figure 7: Top: probability of the system being found in the true minimum for different values of Γ^* , left (right) is lower (higher) noise QPU. Both plots are for a hold time of $\tau = 100 \mu\text{s}$. Values of J_t are colour coded to correspond to the bottom plot. Bottom: peak probability of being in the true minimum for high noise (squares), and low noise (circles) QPUs. Statistical error bars on the upper plots are smaller than the symbols.

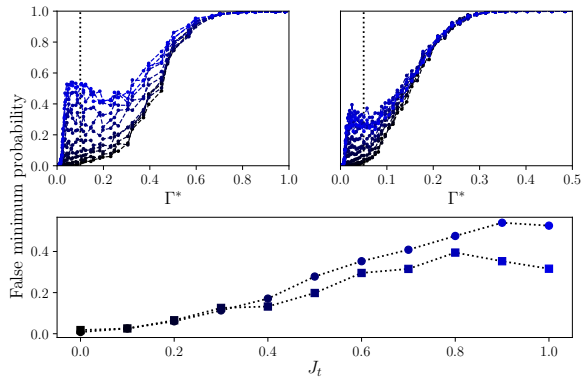


Figure 8: Top: probability of the system being found in the false minimum for different values of Γ^* , left (right) is lower (higher) noise QPU. Both plots are for a hold time of $\tau = 100 \mu\text{s}$. Values of J_t are colour coded in a way which corresponds to the bottom plot. Bottom: maximum probability to be found in the false minimum for $\Gamma \leq 0.1$ ($\Gamma \leq 0.05$) on the lower (higher) noise QPU. As the dashed lines on the top plots show, these values were chosen to capture the initial plateau, before complete transfer into the false minimum.

nelling out of the initial state and tunnelling between the true and false minima. Fig. 9 confirms that at least for a range of Γ values right around the initial peak in true minimum probability, this separation of timescales is a valid assumption, with very little effect on the peak value as hold time is increased.

Based on this separation of timescales we can create a simplified model of the dynamics, in which transfer out of the starting state to the two minima occurs on a very fast timescale, but then transfers from the true minimum to the false minimum occurs on a slower timescale. In this model, we consider an initial transfer which oc-

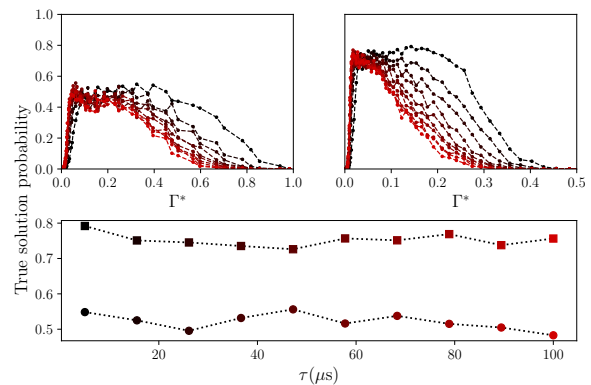


Figure 9: Top: probability of the system being found in the true minimum for different values of Γ^* , left (right) lower (higher) noise QPU. Both plots are for a barrier strength of $J_t = 1$. Values of τ are colour coded in a way which corresponds to the bottom plot. Bottom: peak probability of being in the true minimum for high noise (squares), and low noise (circles) QPUs. Statistical error bars on the upper plots are smaller than the symbols.

curs instantaneously and leaves the system in the false minimum with probability R_{false} , and the true minimum with probability $\simeq (1 - R_{\text{false}})$. After this initial transfer, there is a slow decay from the true minimum into the false minimum, this decay is responsible for the difference in probabilities at different values of hold time τ . Given this separation of timescales, we can directly estimate the branching ratio R_{false} from the initial state into the false minimum for both the lower and higher noise QPUs. To do this, we take data at many values of τ for $s^* = 0.57$ on both the higher and lower noise QPUs. The value of $s^* = 0.57$ was chosen because on one hand even for the smallest τ , this is well above the value of Γ where there is any chance to remain in the initial state, so we are justified in approximating the initial transfer as instantaneous. On the other hand there is still significant probability to be in the true minimum even for the largest value of τ , so the process of transfer between the true and false minima is well captured and can be accurately fit. From these data, we are able to fit the following simplified model

$$P_{\text{false}}(\tau) = 1 - [1 - R_{\text{false}}] \exp(-\kappa\tau) \quad (2)$$

where $P_{\text{false}}(\tau)$ is the probability of being in the false minimum, observed at a given hold time τ . In this simplified model, there is one timescale κ which determines the rate at which amplitude decays from other states (mostly the true minimum) into the the false minimum. As Fig. 10 demonstrates, the branching ratio extracted by fitting does indeed show that the lower noise QPU favours longer range transport of probability amplitude, because it has a larger value of the branching ratio R_{false} for $J_t > 0.4$, i.e., when the barrier height is significant. Although the branching ratio depends on the barrier height, the decay rate κ does not (within errors). This is expected, since

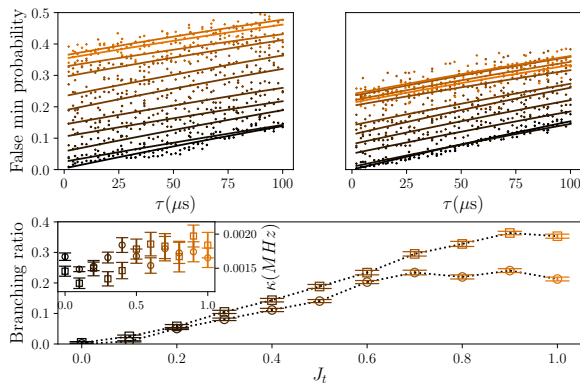


Figure 10: Top: Fits to extract the branching ratio from the initial state to the false minimum at $s^* = 0.57$ corresponding to $\Gamma^* = 0.31$ for the lower noise QPU and $\Gamma^* = 0.089$ for the higher noise QPU. Left (right) is lower (higher) noise QPU. Lines represent the fits, while points represent the individual measurements values of J_t are colour coded in a way which corresponds to the bottom plot. Bottom main: Extracted values of the branching ratios for the higher and lower noise QPUs (R_{false} from Eq. 2). Bottom inset: Extracted values of κ . Circles (squares) represent higher (lower) noise QPU. Error bars are the square root of the variance (i.e. the diagonal elements of the covariance matrix) for each parameter in the non-linear fit. Note that while the statistical error bars on the upper plots are smaller than the symbols, there is clearly some more systematic error present, possibly related to long timescale noise on the device.

there is no obvious mechanism through which the barrier height should have strong effect on the rate of transfer between the true and false minima.

III. METHODS

The experimental data presented in this paper were obtained using using the Matlab API to remotely access the QPUs on September 21st and September 22nd 2019. Numerical analysis and creation of plots was performed in Python [26] using the numpy [27], scipy [28], and matplotlib [29] packages as well as Jupyter notebooks [30]. Data are publicly available [31].

For each raw data point, 1,000 annealing runs were performed. Multiple copies of the gadget were embedded into the QPU for each run, allowing all 11 values of J_t to be annealed simultaneously. A 16×16 chimera graph QPU could accommodate 128 copies of the experimental Hamiltonian, if all qubits were functioning. However, both devices contain a small number of qubits which are non-functional due to failed calibration. For this reason, only 118 total copies of the Hamiltonian were used per run for the higher noise QPU, and 116 for the lower noise QPU. After dividing as evenly as possible over the 11 values of J_t , this still leaves at least 10 copies for each value of J_t on each QPU, and therefore at least 10,000 individual samples for each data point. The standard error for

each data point is therefore **at most 0.5%** (this assuming the worst case scenario of a result which occurs 50% of the time). As this is smaller than the symbols depicted in our plots, statistical error bars resulting from sampling errors have been omitted from all figures. Error bars calculated using different methods are depicted in some figures, as explained in the captions. The definitions of logical 1 and 0 were chosen randomly to avoid systematic errors from uniform fields (this process is sometimes referred to as gauge averaging).

Avoided crossing location and estimated gaps were calculated using numerical bisection on numerically calculated derivatives of the gap. To obtain the gap using reasonable computational resources, the `lobpcg` function (which can be found in `scipy.sparse.linalg`) was used to calculate the gaps. This function takes as inputs estimates of the eigenstates. We used the first 5 eigenstates found at $\Gamma = 1$, using the known state which comprises the true minimum as a sixth state. We have verified by plotting points near the gap location which our bisection has found, that it was not able to fully converge, but is still close enough to the avoided crossing that there is no visible difference between the location it found and the true avoided crossing on the scale plotted in Fig. 4. However, this does mean that the gaps found by bisection should be treated as upper bounds, since they do not lie directly at the crossing. Since tighter bounds on these gaps would not change our interpretation of the experiments, we have elected not to pursue a higher quality estimate.

IV. DISCUSSION AND CONCLUSIONS

In this work, we have presented the results of a small system reverse annealing experiment using an engineered energy landscape, run on D-Wave QPUs which have different noise levels. Our experiment demonstrates the operating principles behind the reverse annealing protocol and verifies that it does indeed perform a local search as predicted in [12]. To our knowledge, this is the most direct demonstration of this behaviour to appear in the literature. More importantly, these experiments have allowed us to examine the effect of reducing the noise on these devices. Crucially, in addition to the expected reduction in dissipation driven state transfer rates, we find that reducing the noise levels results in local searches which are effectively longer range. Since long range quantum tunnelling is necessary for annealers to obtain a quantum advantage, the increase in range which we observe is a positive sign for improving the performance of these devices by reducing noise levels. In the interest of transparency and because re-analysis of our data may be important in understanding open quantum system models of flux qubit quantum devices, we have made our data publicly available [31].

Our results suggest a potential mechanism for the performance improvement associated with reduced noise ob-

served in [23], namely, that noise reduction fundamentally improves the range in solution space over which these devices are able to search. Our results support the evidence in [23] which suggests that reducing noise on flux qubit quantum annealers can provide improved performance on these devices and is therefore important in moving toward a potential quantum advantage. While this may seem like an obvious statement, it is actually far from trivial, as dissipation is actually the driving mechanism behind the currently implemented reverse annealing protocols, and thermal noise has been observed to improve performance [10]. It is therefore not clear whether the best performance could be obtained by removing all coupling to the thermal bath, or whether there is a “sweet spot” where a low (we would speculate still lower than the noise level of the current lowest noise QPUs) but

still significant level of dissipation actually improves device performance. What we can definitely say from our experiments is that the most recent noise reduction has improved an important aspect on the device performance, the range of the local searching, and this therefore suggests that further noise reduction is an interesting route towards device improvement.

Acknowledgments

NC and VK were supported by EP/L022303/1 and impact acceleration funding associated with this grant. NC was supported by EPSRC fellowship EP/S00114X/1.

-
- [1] David Joseph, Adam Callison, Cong Ling, and Florian Mintert. Two quantum Ising algorithms for the shortest vector problem: one for now and one for later. arXiv:2006.14057, 2020. URL <https://arxiv.org/abs/2006.14057>.
- [2] G. E. Coxson, C. R. Hill, and J. C. Russo. Adiabatic quantum computing for finding low-peak-sidelobe codes, 2014. URL <https://doi.org/10.1109/HPEC.2014.7040953>. Presented at the 2014 IEEE High Performance Extreme Computing conference.
- [3] Alejandro Perdomo-Ortiz, Neil Dickson, Marshall Drew-Brook, Geordie Rose, and Alán Aspuru-Guzik. Finding low-energy conformations of lattice protein models by quantum annealing. *Scientific Reports*, 2(1):571, 2012. ISSN 2045-2322. URL <https://doi.org/10.1038/srep00571>.
- [4] T. Stollenwerk, B. O’Gorman, D. Venturelli, S. Mandrá, O. Rodionova, H. Ng, B. Sridhar, E. G. Rieffel, and R. Biswas. Quantum annealing applied to de-conflicting optimal trajectories for air traffic management. *IEEE Transactions on Intelligent Transportation Systems*, 21(1):285–297, 2020. doi: 10.1109/TITS.2019.2891235. URL <https://doi.org/10.1109/TITS.2019.2891235>.
- [5] A. Crispin and A. Syrihas. Quantum annealing algorithm for vehicle scheduling. In *2013 IEEE International Conference on Systems, Man, and Cybernetics*, pages 3523–3528, Oct 2013. doi: 10.1109/SMC.2013.601. URL <http://doi.org/10.1109/SMC.2013.601>.
- [6] Davide Venturelli, Dominic J. J. Marchand, and Galo Rojo. Quantum Annealing Implementation of Job-Shop Scheduling, 2000. URL <https://arxiv.org/abs/quant-ph/1506.08479>. arXiv preprint quant-ph/1506.08479.
- [7] Tony T. Tran, Minh N. Do, Eleanor G. Rieffel, Jeremy Frank, Zhihui Wang, Bryan O’Gorman, Davide Venturelli, and J. Christopher Beck. A hybrid quantum-classical approach to solving scheduling problems. In *SOCS*, 2016. URL <https://www.aaai.org/ocs/index.php/SOCS/SOCS16/paper/view/1395>.
- [8] Daniel O’Malley. An approach to quantum-computational hydrologic inverse analysis. *Scientific Reports*, 8(1):6919, 2018. ISSN 2045-2322. URL <https://doi.org/10.1038/s41598-018-25206-0>.
- [9] Hannes Bernien, Sylvain Schwartz, Alexander Keesling, Harry Levine, Ahmed Omran, Hannes Pichler, Soonwon Choi, Alexander S. Zibrov, Manuel Endres, Markus Greiner, Vladan Vuletić, and Mikhail D. Lukin. Probing many-body dynamics on a 51-atom quantum simulator. *Nature*, 551:579 EP –, 11 2017. URL <https://doi.org/10.1038/nature24622>.
- [10] N. G. Dickson et al. Thermally assisted quantum annealing of a 16-qubit problem. *Nature Communications*, 4(1):1903, 2013. ISSN 2041-1723. URL <https://doi.org/10.1038/ncomms2920>.
- [11] D-Wave Systems Inc. Reverse quantum annealing for local refinement of solutions. https://www.dwavesys.com/sites/default/files/14-1018A-A_Reverse_Quantum_Annealing_for_Local_Refinement_of_Solutions.pdf, 2019. Accessed: 2019-05-03.
- [12] Nicholas Chancellor. Modernizing quantum annealing using local searches. *New Journal of Physics*, 19(2):023024, 2017. doi: 10.1088/1367-2630/aa59c4. URL <https://doi.org/10.1088/1367-2630/aa59c4>.
- [13] Andrew D. King et al. Observation of topological phenomena in a programmable lattice of 1,800 qubits. *Nature*, 560(7719):456–460, Aug 2018. ISSN 1476-4687. doi: 10.1038/s41586-018-0410-x. URL <https://doi.org/10.1038/s41586-018-0410-x>.
- [14] Davide Venturelli and Alexei Kondratyev. Reverse quantum annealing approach to portfolio optimization problems. *Quantum Machine Intelligence*, 1(1):17–30, May 2019. doi: 10.1007/s42484-019-00001-w. URL <https://doi.org/10.1007/s42484-019-00001-w>.
- [15] Daniele Ottaviani and Alfonso Amendola. Low rank non-negative matrix factorization with D-wave 2000Q. arXiv:1808.08721, 2018. URL <https://arxiv.org/abs/1808.08721>.
- [16] John Golden and Daniel O’Malley. Reverse annealing for nonnegative/binary matrix factorization. arXiv:2007.05565, 2020. URL <https://arxiv.org/abs/2007.05565>.
- [17] James King, Masoud Mohseni, William Bernoudy, Alexandre Fréchet, Hossein Sadeghi, Sergei V. Isakov, Hartmut Neven, and Mohammad H. Amin. Quantum-

- assisted genetic algorithm. arXiv:1907.00707, 2019. URL <https://arxiv.org/abs/1907.00707>.
- [18] Adam Callison, Max Festerstein, Jie Chen, Laurentiu Nita, Viv Kendon, and Nicholas Chancellor. An energetic perspective on rapid quenches in quantum annealing. arXiv:2007.11599, 2020. URL <https://arxiv.org/abs/2007.11599>.
- [19] Alejandro Perdomo-Ortiz, Salvador E. Venegas-Andraca, and Alán Aspuru-Guzik. A study of heuristic guesses for adiabatic quantum computation. *Quantum Information Processing*, 10(1):33–52, Feb 2011. ISSN 1573-1332. doi: 10.1007/s11128-010-0168-z. URL <https://doi.org/10.1007/s11128-010-0168-z>.
- [20] Qian-Heng Duan, Shuo Zhang, Wei Wu, and Ping-Xing Chen. An alternative approach to construct the initial Hamiltonian of the adiabatic quantum computation. *Chinese Physics Letters*, 30(1):010302, 2013. doi: 10.1088/0256-307x/30/1/010302. URL <https://doi.org/10.1088/0256-307x/30/1/010302>.
- [21] Tobias Graß. Quantum annealing with longitudinal bias fields. *Phys. Rev. Lett.*, 123:120501, Sep 2019. doi: 10.1103/PhysRevLett.123.120501. URL <https://link.aps.org/doi/10.1103/PhysRevLett.123.120501>.
- [22] R. Harris, M. W. Johnson, S. Han, A. J. Berkley, J. Johansson, P. Bunyk, E. Ladizinsky, S. Govorkov, M. C. Thom, S. Uchaikin, B. Bumble, A. Fung, A. Kaul, A. Kleinsasser, M. H. S. Amin, and D. V. Averin. Probing noise in flux qubits via macroscopic resonant tunneling. *Phys. Rev. Lett.*, 101:117003, Sep 2008. doi: 10.1103/PhysRevLett.101.117003. URL <https://link.aps.org/doi/10.1103/PhysRevLett.101.117003>.
- [23] D-Wave Systems Inc. Improved coherence leads to gains in quantum annealing performance. https://www.dwavesys.com/sites/default/files/14-1037A-A_Improved_coherence_leads_to_gains_QA_performance.pdf, 2019. Accessed: 2020-08-07.
- [24] Sergio Boixo, Tameem Albash, Federico M. Spedalieri, Nicholas Chancellor, and Daniel A. Lidar. Experimental signature of programmable quantum annealing. *Nature Communications*, 4(1):2067, Jun 2013. ISSN 2041-1723. doi: 10.1038/ncomms3067. URL <https://doi.org/10.1038/ncomms3067>.
- [25] D-Wave Systems Inc. Probing mid-band and broadband noise in lower-noise D-Wave 2000Q fabrication stacks. https://www.dwavesys.com/sites/default/files/14-1034A-A_Probing_noise_in_LN_2000Q_fabrication_stacks.pdf, 2019. Accessed: 2019-11-07.
- [26] Guido Van Rossum and Fred L Drake. *Python language reference manual*. Network Theory United Kingdom, 2003.
- [27] Travis E Oliphant. *A guide to NumPy*, volume 1. Trelgol Publishing USA, 2006.
- [28] Eric Jones, Travis Oliphant, Pearu Peterson, et al. SciPy: Open source scientific tools for Python, 2001–. URL <http://www.scipy.org/>. [Online; accessed March 22, 2022].
- [29] John D Hunter. Matplotlib: A 2D graphics environment. *Computing in science & engineering*, 9(3):90, 2007.
- [30] Thomas Kluyver, Benjamin Ragan-Kelley, Fernando Pérez, Brian Granger, Matthias Bussonnier, Jonathan Frederic, Kyle Kelley, Jessica Hamrick, Jason Grout, Sylvain Corlay, Paul Ivanov, Damián Avila, Safia Abdalla, and Carol Willing. Jupyter notebooks – a publishing format for reproducible computational workflows. In F. Loizides and B. Schmidt, editors, *Positioning and Power in Academic Publishing: Players, Agents and Agendas*, pages 87 – 90. IOS Press, 2016.
- [31] Nicholas Chancellor and Viv Kendon. Data and code associated with: search range in experimental quantum annealing. **Public repository to be posted, link will appear in a later arXiv version.**
- [32] A table of parameter values at different values of s for each device is provided to all QPU users.